

Improved Mesoporous Structure of High Surface Area Carbon Nanofiber for Electrical Double-Layer Capacitors

Young-Geun Lee¹, Geon-Hyoung An² and **Hyo-Jin Ahn**^{1,2†}

¹Department of Materials Science and Engineering, Seoul National University of Science and Technology, Seoul 01811, Republic of Korea

²Program of Materials Science & Engineering, Convergence Institute of Biomedical Engineering and Biomaterials, Seoul National University of Science and Technology, Seoul 01811, Republic of Korea

(Received February 14, 2017 : Revised March 8, 2017 : Accepted March 10, 2017)

Abstract Carbon nanofiber (CNF) is used as an electrode material for electrical double layer capacitors (EDLCs), and is being consistently researched to improve its electrochemical performance. However, CNF still faces important challenges due to the low mesopore volume, leading to a poor high-rate performance. In the present study, we prepared the unique architecture of the activated mesoporous CNF with a high specific surface area and high mesopore volume, which were successfully synthesized using PMMA as a pore-forming agent and the KOH activation. The activated mesoporous CNF was found to exhibit the high specific surface area of $703 \text{ m}^2 \text{ g}^{-1}$, total pore volume of $0.51 \text{ cm}^3 \text{ g}^{-1}$, average pore diameter of 2.9 nm, and high mesopore volume of 35.2 %. The activated mesoporous CNF also indicated the high specific capacitance of 143 F g^{-1} , high-rate performance, high energy density of $17.9\text{-}13.0 \text{ Wh kg}^{-1}$, and excellent cycling stability. Therefore, this unique architecture with a high specific surface area and high mesopore volume provides profitable synergistic effects in terms of the increased electrical double-layer area and favorable ion diffusion at a high current density. Consequently, the activated mesoporous CNF is a promising candidate as an electrode material for high-performance EDLCs.

Key words electrical double layer capacitors, carbon nanofiber, high surface area, mesopore, micropore.

1. Introduction

Owing to their higher power density, faster charge/discharge rates, good cycling stability, and wide operating temperature range, electrochemical capacitors are among the most desirable energy storage devices.¹⁻⁵⁾ Consequently, electrochemical capacitors have been widely applied in various applications, such as electric vehicles, air bags, black box, and memory back-up devices.^{6,7)}

In general, electrochemical capacitors can be classified into two types: electrical double-layer capacitors (EDLCs) and pseudocapacitors. EDLCs can garner charge using the capacitive process, which mobilizes the charge separation between the electrode and electrolyte interface.⁸⁻¹⁰⁾ On the other hand, pseudocapacitors use the redox reactions that involve the reversible electron-exchange process between the electrode and the electrolyte interface.⁸⁻¹⁰⁾ Due to their high power density, low fabrication cost, high-

rate performance, and superb cycling stability and despite their relatively lower specific capacitance, as compared with pseudocapacitors, EDLCs have been most used in the industry field.

EDLCs are composed of three main parts: the carbon-based electrode, the electrolyte, and the separator. Among these, the specific capacitance of EDLCs is mainly determined by the carbon-based electrode. Various carbon materials, such as activated carbon, graphene, carbon nanotube, and carbon nanofiber (CNF), have been investigated as electrode materials for EDLCs.¹¹⁻¹⁹⁾ Of these, owing to its attractive advantages, such as high surface areas ($359 \text{ m}^2 \text{ g}^{-1}$), high aspect ratios, excellent chemical and physical stability, and network structure for an efficient electron transport, CNF is an indispensable candidate as an electrode material for EDLCs.¹¹⁻¹⁹⁾ To enhance the electrochemical performance of EDLCs, the CNF structure should possess a high surface area, high mesopore volume, high

[†]Corresponding author

E-Mail : hjahn@seoultech.ac.kr (H.-J. Ahn, Seoul Nat'l Univ. Sci. Technol.)

© Materials Research Society of Korea, All rights reserved.

This is an Open-Access article distributed under the terms of the Creative Commons Attribution Non-Commercial License (<http://creativecommons.org/licenses/by-nc/3.0>) which permits unrestricted non-commercial use, distribution, and reproduction in any medium, provided the original work is properly cited.

electrical conductivity, and good electrochemical stability.^{13,16,17} Among these characteristics, the high surface area is the most significant in terms of gaining the increased specific capacitance. Thus, in order to increase the surface area with micropores of CNFs, the potassium hydroxide (KOH) activation is used. The KOH activation has several advantages, such as effortless process, cost effectiveness, and large-scale production.²⁰⁻²² Moreover, the high-rate performance is also a very significant factor, because EDLCs are generally applied in high-power applications.^{16,23} The high mesopore volume of CNF can expect the shorter diffusion routes and low resistance pathways for ions, leading to an enhanced high-rate performance.^{24,25} However, a combined research of high surface area and high mesopore volume with similar CNF diameters is still not enough for high-performance EDLCs.

Thus, in the present study, we prepared an improved mesoporous structure of the activated CNF with a high surface area; the material was synthesized by electrospinning and carbonization with the KOH activation. To increase the surface of CNF, the KOH activation was introduced during the carbonization process. In addition, the pore-forming agent was injected in the electrospinning solution to improve the mesopore volume in CNF. This unique architecture permits the high surface area and high mesopore volume of CNF. We also examined the relationship between the surface features and the electrochemical properties for high-performance EDLCs.

2. Experimental Procedure

2.1 Chemicals

Polyacrylonitrile (PAN, $M_w = \sim 150,000$), Poly (methyl methacrylate) (PMMA, $M_w = \sim 120,000$), and N,N-dimethylformamide (DMF, 99.8 %) were purchased from Sigma-Aldrich. Potassium hydroxide (KOH) was purchased from SAMCHUN. All chemicals were used without further purification.

2.2 Synthesis of the improved mesoporous structure of carbon nanofiber with high surface area

The improved mesoporous structure of CNF with a high surface area (the activated mesoporous CNF) was successfully fabricated using PMMA as the pore-forming agent and the KOH activation. First, 10.0 wt% PAN and 0.5 wt% PMMA were dissolved in DMF under vigorous stirring for 5 h. Then, PMMA was used to develop the mesopores of CNF. For the electrospinning process, the voltage and the feed rate were fixed at 13 kV and 0.03 mL h⁻¹, respectively. The syringe needle-to-collector distance and humidity in the chamber were set at ~ 15 cm and under 20 %, respectively. Thereafter, the as-spun nanofibers were stabilized at 270 °C for 2 h in air. The

stabilized nanofibers were mixed with KOH and carbonized at 800 °C for 2 h in nitrogen atmosphere. Finally, the resultant sample was washed several times with deionized water and hydrochloric acid, which was dried at 80 °C in an oven. In addition, for comparison, we also prepared the activated carbon nanofiber with a high surface area without the improvement of mesoporous structure (the activated CNF) and the mesoporous carbon nanofiber without the KOH activation (the mesoporous CNF).

2.3 Characterization

The structures of the samples were examined by field emission-scanning electron microscopy (FE-SEM, Hitachi S-4800) and transmission electron microscopy (MULTI/TEM; Tecnai G², KBSI Gwangju Center). The crystal structures of the samples were characterized by X-ray diffractometry (XRD, Rigaku D/Max 2500 V) with the Cu K α radiation in the range from 10° to 90°. The contents were determined by the thermogravimetric analysis (TGA-50, Shimadzu) in the temperature range from 200 °C to 800 °C at the heating rate of 10 °C min⁻¹ in air. The surface properties, such as specific surface area, average pore diameter, and total pore volume, were characterized by the Brunauer-Emmett-Teller (BET) and Barrett-Joyner-Halenda (BJH) methods using N₂ adsorption at 77 K.

2.4 Preparation of electrodes and electrochemical characterization

Electrochemical measurements were performed using a symmetric two-electrode system with nickel foam as the substrate and a 6 M KOH solution as the electrolyte. The paste, which consisted of 70 wt% prepared samples, 20 wt% poly (vinylidene difluoride) (PVDF) as a binder, and 10 wt% Ketjen black (Mitsubishi Chemical, ECP-600JD) as a conducting material in N-methyl-2-pyrrolidinone (NMP, 99.5 %), was coated on nickel foams and dried in air at 80 °C for 12 h. The mass of prepared sample was optimized 2.35 mg cm⁻². Cyclic voltammetry (CV) measurements were performed using a potentiostat/galvanostat (Autolab PGSTAT302N, FRA32M) at the scan rate of 10 mV s⁻¹ in the potential range of 0.0-1.0 V. The galvanostatic charging/discharging tests were performed at the current density of 0.1-20 A g⁻¹ in the voltage range of 0.0-1.0 V using a cycler system (Won-A Tech., WMPG 3000). The cycling stability of the electrodes was investigated at the current density of 1 A g⁻¹ up to 500 cycles.

3. Results and discussion

Fig. 1 shows a schematic illustration of the synthetic process of the activated mesoporous CNF. As shown in Fig. 1a, the PAN and PMMA nanofiber was prepared by electrospinning. To obtain the high surface area of CNF,

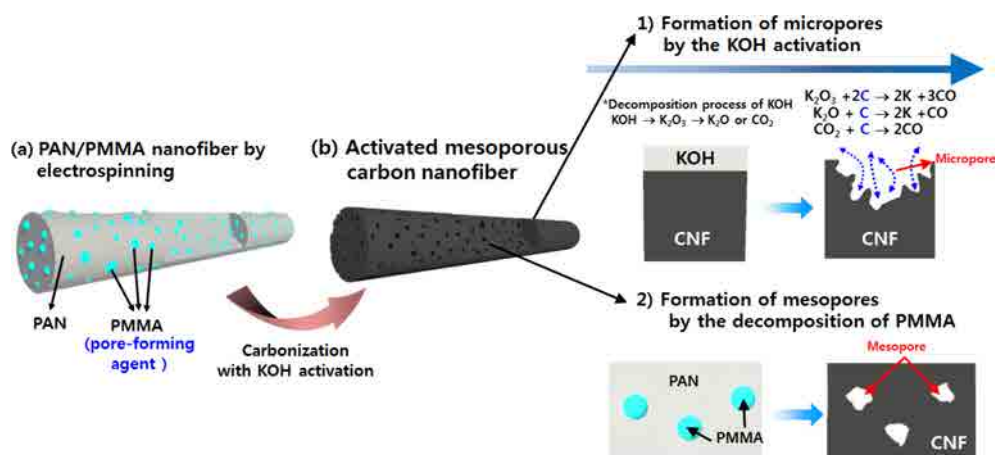


Fig. 1. Schematic illustration for the synthetic process of the activated mesoporous CNF.

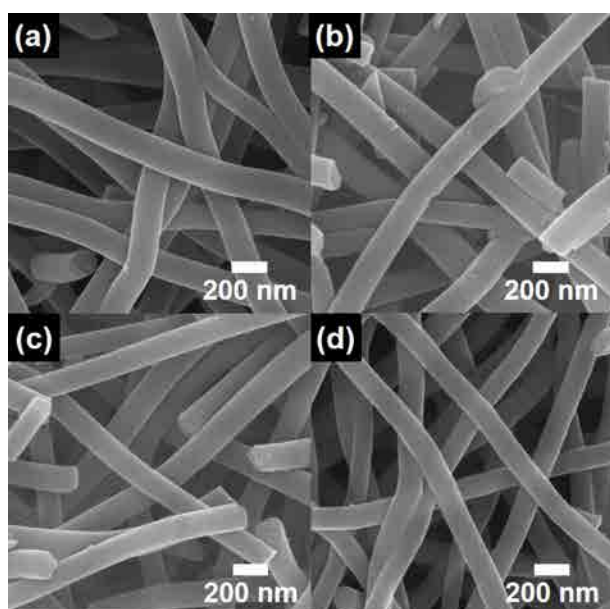


Fig. 2. The FESEM images of (a) CNF, (b) the activated CNF, (c) mesoporous CNF, and (d) activated mesoporous CNF.

the KOH activation was used during carbonization. The activation process can be accounted for by the decomposition process of KOH: $\text{KOH} + \text{C} \rightarrow \text{K} + \text{H}_2 + \text{K}_2\text{CO}_3$. Subsequently, K_2CO_3 decomposes into CO_2 , and O_2 , leading to the activation of CNF.^{26,27)} In addition, PMMA was used as the pore-forming agent in the electrospinning solution to improve the mesoporous structure of CNF. Thus, an activated mesoporous CNF (Fig. 1b) was fabricated by electrospinning and carbonization with the KOH activation.

Fig. 2 shows the SEM images of CNF, the activated CNF, mesoporous CNF, and activated mesoporous CNF. All samples displayed uniform morphologies and smooth surfaces, presenting a linked network structure composed

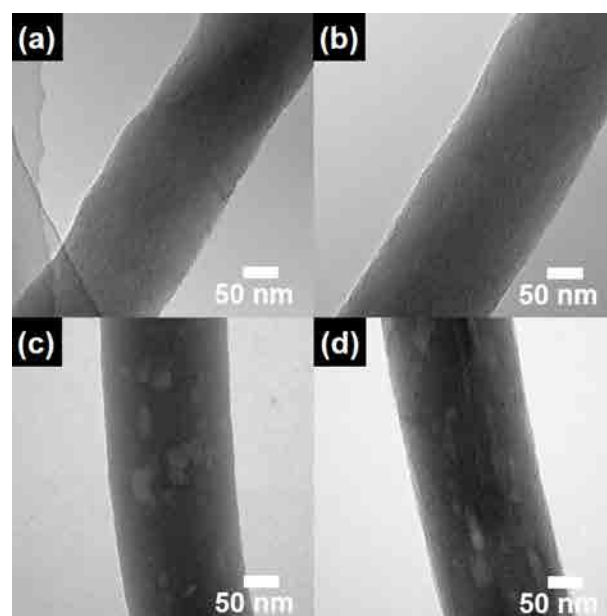


Fig. 3. The TEM images of (a) CNF, (b) the activated CNF, (c) mesoporous CNF, and (d) activated mesoporous CNF.

of the one-dimensional nanofiber structure. This network structure can plainly provide an efficient electron transfer and a rapid ion diffusion rate during cycling, leading to a high performance of EDLCs. The similar diameters of the all nanofibers were found to be 203~227 nm. Thus, we prepared the similar diameters of CNF as electrode materials for comparing the electrochemical performance in EDLCs.

The TEM measurements were performed to further investigate the structural properties of the samples (see Fig. 3). Due to a single carbon phase, CNF (Fig. 3a) and the activated CNF (Fig. 3b) displayed uniform brightness along their bodies, indicating that the KOH activation developed the only micropores with a high surface area.

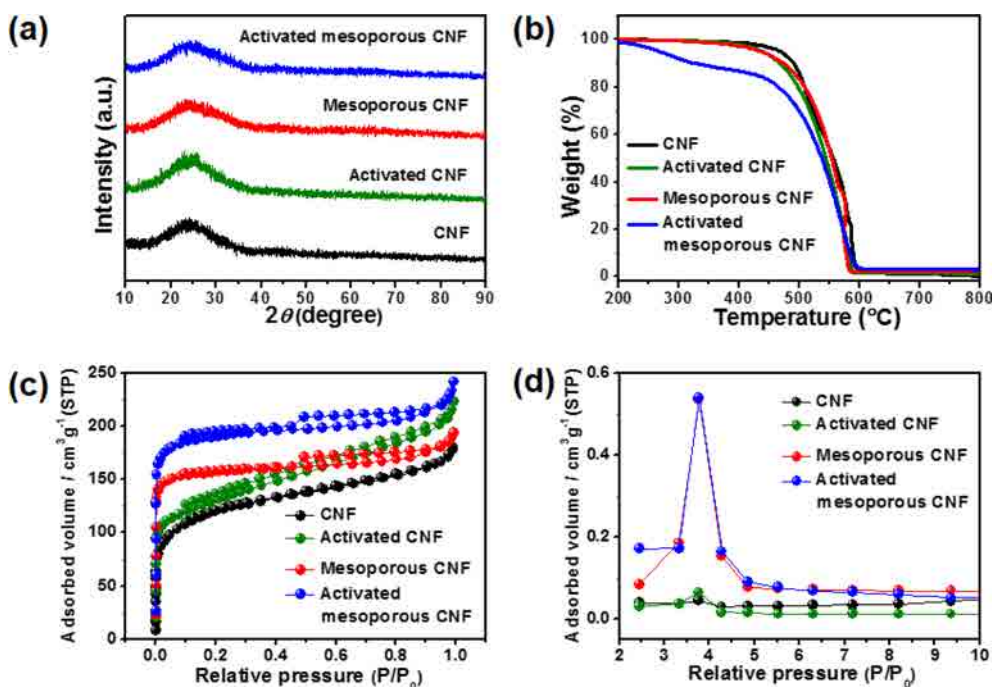


Fig. 4. (a) The XRD data, (b) the TGA curves, (c) N_2 adsorption/desorption isotherms, and (d) the BJH pore size distributions of CNF, the activated CNF, mesoporous CNF, and activated mesoporous CNF.

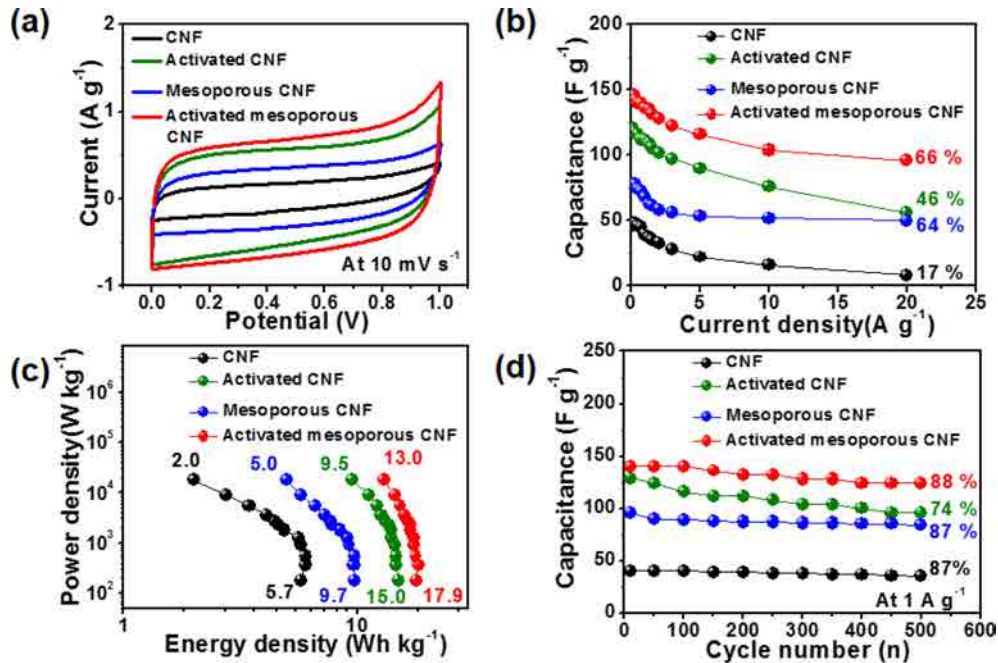
On the other hand, owing to the existence of small pores within the CNF, the mesoporous CNF (Fig. 3c) showed non-uniform brightness along their bodies. These results imply that the mesopores in CNF were formed by the decomposition of PMMA as the pore-forming agent during the carbonization process.²¹⁾ Accordingly, the activated mesoporous CNF (see Fig. 3d) showed the mesoporous structure. Thus, the improved mesoporous structure of CNF could provide shorter diffusion routes and low resistance pathways for ions, leading to a high-rate performance of EDLCs.

Fig. 4a shows the XRD data to investigate their crystal structures. All samples showed broad diffraction peaks at around 25° , corresponding to the (002) layers of graphite.²⁸⁻³⁰⁾ These results imply that the crystal structure of all samples did not change by the usage of PMMA as the pore-forming agent and the KOH activation. As shown in Fig 4b, TGA was conducted in the temperature range from 200°C to 800°C at the heating speed of $10^\circ\text{C min}^{-1}$ in air. All samples indicated a weight loss of 100%, implying the existence of pure carbon without impurities. In addition, the activated mesoporous CNF showed a quick weight loss at the low temperature area, which means a high reaction area between the carbon and air. To explore the surface behaviors and pore structures, N_2 adsorption/desorption isotherms were investigated by the BET measurements (see Fig. 4c). The isotherm of CNF and the activated CNF exhibits type I characteristics,

based on the international union of pure and applied chemistry (IUPAC) nomenclature, signifying the presence of microporous pores (width $< 2\text{ nm}$) at relatively low pressures ($P/P^0 < 0.1$) in CNF.^{7,16)} On the other hand, the isotherm of the mesoporous CNF and activated mesoporous CNF presents mixed characteristics of types I and IV, suggesting the existence of mesoporous pores (width $2\text{-}50\text{ nm}$) at a relatively intermediate pressure ($P/P^0 = 0.5$) in CNF.^{7,16)} The detailed information on the specific surface area, total pore volumes, average pore diameters, and the pore volume of the samples is summarized in Table 1. The specific surface area of the activated mesoporous CNF ($703\text{ m}^2\text{ g}^{-1}$) is 2.0, 1.1, and 1.3 times higher than that of CNF, the activated CNF, and the mesoporous CNF, respectively. In addition, the activated mesoporous CNF indicates the high mesopore volume of 35%, as compared to CNF and activated CNF. Thus, the usage of PMMA in the PAN nanofiber improves the mesopore volume, whereas the KOH activation only provides a high surface area with micropores. Fig. 4d shows the BJH measurements to investigate the pore volumes and the pore size distributions in the mesopore size range of $2\text{-}10\text{ nm}$. The activated mesoporous CNF displays a high mesopore volume, as compared to CNF and the activated CNF. Therefore, the BET and BJH results show that, due to the combined effects of PMMA in PAN nanofiber and KOH activation, the activated mesoporous CNF obtained a high mesopore volume and a high surface

Table 1. List of the specific surface area, total pore volumes, average pore diameters, and the pore volume.

Samples	S_{BET} [$\text{m}^2 \text{g}^{-1}$]	Total pore volume ($p/p_0 = 0.990$) [$\text{cm}^3 \text{g}^{-1}$]	Average pore diameter [nm]	Pore volume	
				V_{micro} (%)	V_{meso} (%)
CNF	353	0.1	1.9		88.5
Activated CNF	615	0.3	1.9		87.7
Mesoporous CNF	522	0.3	2.8		64.7
Activated mesoporous CNF	703	0.5	2.8		64.8

**Fig. 5.** (a) Cyclic voltammetry (CV) measurements of CNF, activated CNF, mesoporous CNF, and activated mesoporous CNF at the scan rate of 10 mV s^{-1} in the voltage range of 0.0-1.0 V. (b) Specific capacitance at the current density of 0.1-20 A g^{-1} . (c) Ragone plot in the power density range from 180-18000 W kg^{-1} . (d) Cycling durability at the current density of 1 A g^{-1} up to 500 cycles.

area, respectively, which could be useful in high-performance EDLCs.

Fig. 5a shows the CV curves of all samples at the scan rate of 10 mV s^{-1} in the voltage range of 0.0-1.0 V in 6 M KOH aqueous electrolyte. Compared to other electrodes, the activated mesoporous CNF electrode displays the largest rectangular ideal CV curve, implying an increased electrical double-layer area resulting from the high specific surface area. The specific capacitance (C_{sp}) of the electrodes was evaluated at the current density of 0.1-20 A g^{-1} using Eq. (1).^{11,16,20}

$$C_{\text{sp}} = 4I/(m dV/dt) \quad (1)$$

where I (A) is the current, m (g) is the total mass of the active material, dV is the voltage window, and dt (s) is the total discharging time. As shown in Fig. 5b, the specific capacitances of CNF, the activated CNF, mesoporous

CNF, and activated mesoporous CNF electrodes at the current density of 0.1 A g^{-1} were 46, 120, 78, and 143 F g^{-1} , respectively. CNF electrode exhibited a typical specific capacitance of CNF-based electrode.^{7,11,16} As compared to CNF, the activated CNF electrode showed an improved specific capacitance of 120 F g^{-1} , indicating that an increased surface area could provide a high electrical double-layer area, leading to the enhanced specific capacitance in EDLCs. However, as compared with the activated CNF and the activated mesoporous CNF electrodes, the mesoporous CNF electrode displayed a relatively low specific capacitance of 78 F g^{-1} owing to the relatively low surface area. Of note, the activated mesoporous CNF electrode exhibited mainly a highest specific capacitance of 143 F g^{-1} due to the highest surface area, as compared to other electrodes, implying the increased electrical double-layer area between the electrode and the electrolyte. With an increase of the current

density, the specific capacitance decreased slightly because of the reduced ion diffusion time during the charge/discharge cycling. Nevertheless, the activated mesoporous CNF electrode showed an excellent high-rate performance with the specific capacitance of 96 F g^{-1} even at the high current density of 20 A g^{-1} . These results suggest that a high mesopore volume could furnish shorter diffusion routes and low resistance pathways for ions, leading to an improved high-rate performance. Thus, we believe that the improved electrochemical performance, including specific capacitance and high-rate performance, can mainly be ascribed to the following two aspects: (1) the enhanced specific capacitance can be attributed to the high surface area of CNF related to the increased electrical double-layer area between the electrode and the electrolyte; (2) the improved high-rate performance can be attributed to the high mesopore volume of CNF related to the accessible diffusion of ions at a high current density.

In the Ragone plot (see Fig. 5c), the power density (P , W kg^{-1}) and energy density (E , Wh kg^{-1}) were calculated using charge and discharge measurements using Eq. (2-3).^{11,16,21)}

$$E = C_{sp}V^2/8 \quad (2)$$

$$P = E/dt \quad (3)$$

where C_{sp} , V , and dt are the specific capacitance, the discharge voltage, and the discharge time, respectively. Consequently, the Ragone plots display a reduction of the energy density with an increasing power density. The highest energy density of the activated mesoporous CNF electrode presented $17.9\text{-}13.0 \text{ Wh kg}^{-1}$ in the power density range from $180\text{-}18000 \text{ W kg}^{-1}$. Fig. 5d indicates the cycling stability for all electrodes measured at the current density of 1 A g^{-1} up to 500 cycles. The activated mesoporous CNF electrode exhibited an excellent cycling stability with the specific capacitance retention of 88%. These results can be ascribed to a high mesopore volume related to favourable ion diffusion, as well as to the network structure of CNF with an efficient electron transport.^{7,13,16)} However, as compared to the activated mesoporous CNF, the activated CNF showed a relatively poor cycling stability with the specific capacitance retention of 74%, which was due to the low mesopore volume. Therefore, the cycling stability of EDLCs depends on the mesopore volume of CNF.

In the present study, we demonstrated that the improved electrochemical performance of the activated mesoporous CNF electrode can be elucidated as follows: (1) a high surface area could enhance specific capacitance because of the increased electrical double-layer area between the electrode and the electrolyte; (2) a high mesopore

volume could improve a high-rate performance and result in an excellent cycling stability relative to the favorable ion diffusion at a high current density. The mesoporous structure could provide shorter ion diffusion routes and low resistance pathways for the ions using the mesopores.

4. Conclusions

In the present study, the activated mesoporous CNF with a high specific surface area and high mesopore volume have been successfully fabricated using PMMA as the pore-forming agent and the KOH activation and their electrochemical performance in EDLCs has been demonstrated. The activated mesoporous CNF showed the high specific surface area of $703 \text{ m}^2 \text{ g}^{-1}$, total pore volume of $0.51 \text{ cm}^3 \text{ g}^{-1}$, average pore diameter of 2.9 nm , and high mesopore volume of 35.2%. The KOH activation provided a high surface area with micropores. In addition, PMMA as the pore-forming agent in the PAN nanofiber improved the mesopore volume. The activated mesoporous CNF also indicated the high specific capacitance of 143 F g^{-1} at the current density of 0.1 A g^{-1} , high-rate performance, high energy density of $17.9\text{-}13.0 \text{ Wh kg}^{-1}$, and outstanding cycling stability. The improved electrochemical performance of EDLCs can be explained by two main effects. First, the high surface area related to the electrical double-layers developed on the surface has led to a high specific capacitance. Second, the high mesopore volume improved ion diffusion related to shorter diffusion routes and low resistance pathways for ions, leading to an outstanding high-rate performance and a superb cycling stability. Thus, we conclude that the unique architecture of the activated mesoporous CNF using PMMA as the pore-forming agent and the KOH activation has a remarkable potential as an electrode material in EDLCs.

Acknowledgments

This research was supported by Basic Science Research Program through the National Research Foundation of Korea (NRF) funded by the Ministry of Science, ICT and Future Planning (NRF-2015R1A1A1A05001252).

References

1. P. Simon, Y. Gogotsi and B. Dunn, *Science*, **343**, 1210 (2014).
2. P. Simon and Y. Gogotsi, *Nat. Mater.*, **7**, 845 (2008).
3. M. Inagaki, H. Konno and O. Tanaike, *J. Power sources*, **195**, 7880 (2010).
4. Y. J. Lee, G. H. An and H. J. Ahn, *Korea J. Mater. Res.*, **24**, 37 (2014).
5. T. D. Nguyen, J. K. Ryu, B. S. N and T. N. Kim, *Korea*

- J. Mater. Res., **23**, 643 (2013).
6. G. H. An and H. J. Ahn, ECS Solid State Lett., **2**, M33 (2013).
 7. G. H. An and H. J. Ahn, Carbon, **65**, 87 (2013).
 8. I. Yang, G. Lee and J. C. Jung, Korean J. Mater. Res., **26**, 696 (2016).
 9. E. Lee, S. H. Kwon, P. Choi, J. C. Jung and M. S. Kim, Korea J. Mater. Res., **24**, 285 (2014).
 10. Y. Luan, Y. Huang, L. Wang, M. Li, R. Wang and B. Jiang, J. Electroanal. Chem., **763**, 90 (2016).
 11. G. H. An and H. J. Ahn, J. Electroanal. Chem., **744**, 32 (2015).
 12. G. H. An, J. I. Sohn and H. J. Ahn, J. Mater. Chem. A, **4**, 2049 (2016).
 13. B. H. Kim and K. S. Yang, J. Electroanal. Chem., **714-715**, 92 (2014).
 14. B. H. Kim, C. H. Kim and D. G. Lee, J. Electroanal. Chem., **760**, 64 (2016).
 15. G. H. An, E. H. Lee and H. J. Ahn, J. Alloys Compd., **682**, 746 (2016).
 16. G. H. An, B. R. Koo and H. J. Ahn, Phys. Chem. Chem. Phys., **18**, 6587 (2016).
 17. D. P. Upare, S. Yoon and C. W. Lee, Korean J. Chem. Eng., **28**, 731 (2011).
 18. G. H. An and H. J. Ahn, J. Power sources, **272**, 828 (2014).
 19. G. H. An, D. Y. Lee, Y. J. Lee and H. J. Ahn, ACS Appl. Mater. Inter., **8**, 30264 (2016).
 20. G. Yu, X. Xie, L. Pan, Z. Bao and Y. Cui, Nano Energy, **2**, 213 (2013).
 21. J. Y. Hong, J. J. Wie, Y. Xu and H. S. Park, Phys. Chem. Chem. Phys., **17**, 30946 (2015).
 22. Y. Huang, J. Liang and Y. Chen, Small, **8**, 1805 (2012).
 23. G. H. An, H. J. Ahn and W. K. Hong, J. Power Sources, **274**, 536 (2015).
 24. B. H. Kim, K. S. Yang and J. P. Ferraris, Electrochim. Acta, **75**, 325 (2012).
 25. G. H. An, D. Y. Lee and H. J. Ahn, ACS Appl. Mater. Inter., **8**, 19466 (2016).
 26. J. Wang and S. Kaskel, J. Mater. Chem., **22**, 23710 (2012).
 27. Y. Ji, T. Li, L. Zhu, X. Wang and Q. Lin, Appl. Surf. Sci., **254**, 506 (2007).
 28. J. W. Lang, X. B. Yan, W. W. Liu, R. T. Wang and Q. J. Xue, J. Power Sources, **204**, 220 (2012).
 29. G. H. An and H. J. Ahn, Ceram. Int., **38**, 3197 (2012).
 30. G. H. An and H. J. Ahn, ECS Solid State Lett., **3**, M29 (2014).